High-Gain Holographic Multi-Feed Antenna

Maximilian Döring, Thomas Frey, Christian Waldschmidt, Tobias Chaloun
University Ulm, Institute of Microwave Engineering, Germany
maximilian.doering@uni-ulm.de

***Abstract*— In this work, a novel multi-feed synthesis for holographic leaky-wave (LW) antennas is presented that considers the angular dependence of each pixel structure. This approach of combining multiple single-beam holograms minimizes the impedance error w.r.t. each individual impedance hologram. A multi-feed antenna with two feeding points at 20 GHz is fabricated and measured using this new design methodology. The simulation and measurement results show a good agreement. The fabricated LW antenna has a gain of 21.7 dBi and 22.1 dBi and a side lobe level (SLL) of 9.0 dB and 9.6 dB for both feeds.**

***Keywords*— holographic antenna, multi-feed antenna, high gain**

I. Introduction

In the last decades, the interest in holographic antennas has strongly grown, mainly because of the high flexibility of amplitude, phase, and polarization control [1]. Thus, this type of antenna serves a wide range of applications. In recent years, various types of holographic leaky-wave (LW) antennas have been published [2], [3], [4]. These works emphasis on the design of single-beam antennas. However, many sensor and communication applications require multiple beams. This leads to the challenge of combining multiple impedance holograms, which corresponds to multiple feeds, on one shared antenna aperture. A concepts for multi-beam holographic antennas is introduced in [5], where an arithmetic averaging is used to merge the impedance holograms. However, an averaging of all impedance holograms does not take into account the incident angle dependency of the surface wave (SW) from the respective feeding point. In this contribution, a novel multi-feed synthesis is presented that considers the angular dependence for each individual feeding point, which minimizes the deviation of the combine impedance hologram to the individual ones. Additionally, a genetic algorithm optimization is used that exploits the degree of freedom in positioning the feeds.

II. Hologram Synthesis

In general, the following hologram synthesis can be performed for N feeds; for the sake of simplicity the synthesis process is discussed using two feeds only. Applying an impedance boundary condition (IBC), an anisotropic impedance tensor for each feed relates a given current and electric field on the aperture plane:

$$\underline{\vec{E}}_{\text{obj},n} = \underline{\overleftrightarrow{Z}}_n \cdot \underline{\vec{J}}_{\text{surf},n} - \underline{\vec{E}}_{\text{WR},n} \;\forall\, n \in \mathbb{N}\,, \tag{1}$$

where $\underline{\vec{E}}_{\text{WR},n}$ defines the electric field distribution of the weakly radiating modes for each feed [2]. The surface current

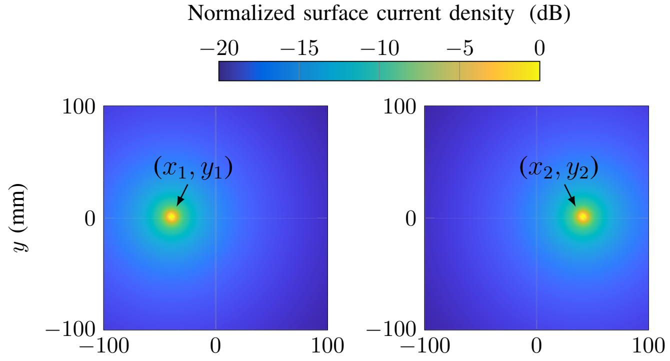

(a) $\underline{\vec{J}}_{\text{surf},1}$ (b) $\underline{\vec{J}}_{\text{surf},2}$

Fig. 1. Surface current density on the antenna aperture for feed 1 (x_1, y_1) and feed 2 (x_2, y_2) at 20 GHz.

density $\underline{\vec{J}}_{\text{surf},n}$ of each feed is excited by a radial propagating TM_0 surface wave mode on the antenna aperture and is defined as:

$$\underline{\vec{J}}_{\text{surf},n}(x,y) = \vec{e}_z \times \left(\begin{pmatrix} \cos\phi \\ -\sin\phi \end{pmatrix} \underline{I}_{\text{TM}_0} H^{(2)}_{1,n}(x,y) \right) \forall\, n \in \mathbb{N}\,, \tag{2}$$

where $H^{(2)}_{1,n}$ is the Hankel function of the second kind and first order. This expresses the decay behavior of the current distribution and is depicted in Fig. 1 for two exemplary feed positions (x_1, y_1) and (x_2, y_2). The term $\underline{I}_{\text{TM}_0}$ is the complex excitation coefficient of the SW and $\vec{e}_z$ is the unit vector in z-direction. The angle ϕ defines the azimuth in the aperture plane of the antenna. The tangential objective electric field is formulated for the n-th feed

$$\underline{\vec{E}}_{\text{obj},n}(x,y) = \begin{pmatrix} E_{x_0,n} \mathrm{e}^{-\mathrm{j}(k_{x,n}x)}\, T_{x,n}(x,y) \\ E_{y_0,n} \mathrm{e}^{-\mathrm{j}(k_{y,n}y+\varphi_y)}\, T_{y,n}(x,y) \end{pmatrix} \;\forall\, n \in \mathbb{N}\,, \tag{3}$$

where $\vec{T}_n$ describes the amplitude taper function on the aperture. The phase distribution is set by the exponential function in (3). With $\varphi_y = \mp\frac{\pi}{2}$, a right-handed circular polarization (RHCP) or a left-handed circular polarization (LHCP) is defined, respectively. Both the amplitude and the phase of $\underline{\vec{E}}_{\text{obj},n}$ corresponds to the far field pattern for the n-th feed through an inverse discrete Fourier transformation (IDFT). According to (3), Figs. 2(a) and 2(c) illustrate the amplitude and phase of the objective field for feed 1. The amplitude follows a Taylor distribution, and the phase progression results from a defined elevation angle $\vartheta_{0,1} = -10°$ w.r.t. boresight.

ISBN 978-3-9820397-2-5

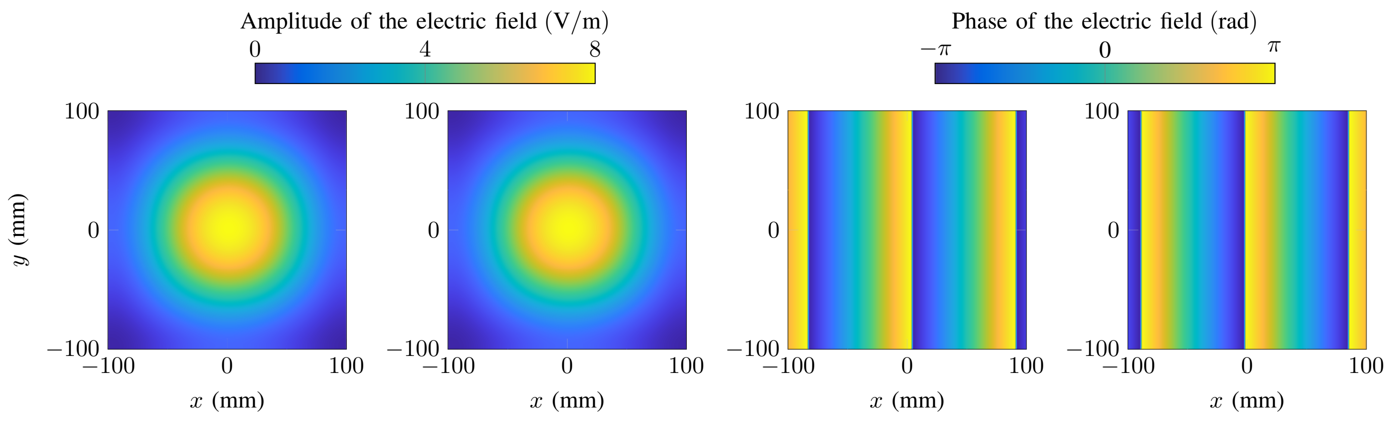

(a) $|\vec{\underline{E}}_{\text{obj},1}|$ (b) $|\vec{\underline{E}}_{\text{obj},2}|$ (c) $\varphi_{\text{Eobj},1}$ (d) $\varphi_{\text{Eobj},2}$

Fig. 2. Analytical calculation of the objective electric field distribution on the antenna aperture at 20 GHz. (a) and (c) amplitude and phase of feed 1 and (b),(d) amplitude and phase of feed 2.

Feed 2 has the same amplitude distribution as feed 1 but a different elevation angle in the elevation plane $\vartheta_{0,2} = 10°$ leading to a different phase progression as shown in Fig. 2(d). With the IBC from (1), the impedance tensors $\overleftrightarrow{\underline{Z}}_1$ and $\overleftrightarrow{\underline{Z}}_2$ can be derived. These can be transformed into an incident angle dependent scalar impedance $\underline{Z}_{s,1}$, $\underline{Z}_{s,2}$ by solving an eigenvalue problem [6]. The resulting scalar impedance hologram for each feed is shown in Fig. 3. Without loss of generality, in this contribution an RHCP radiation is realized and thus, both impedance holograms have a spiral-like shape. If only a single-feed antenna is synthesized, the impedance hologram of either feed 1 or feed 2 could be realized on the antenna aperture. However, for the realization of the discussed multi-feed antenna, two holograms are intended to share the same aperture. This merging of two impedance holograms causes deviations from the ideal ones and thus leads to errors in their synthesized objective electric fields. Therefore, a merging algorithm has to be applied that aims to minimize the deviations of the shared impedance hologram w.r.t the individual ones.

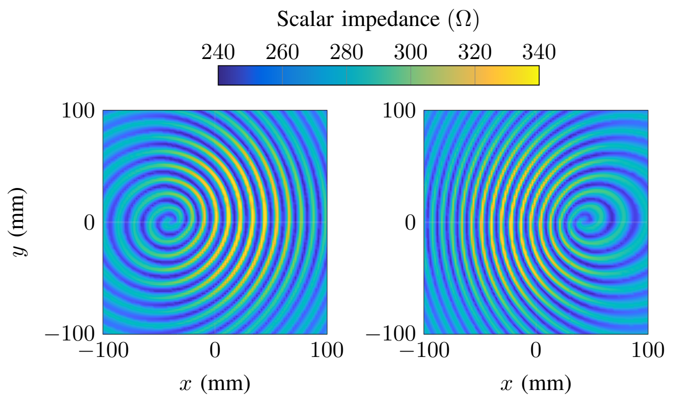

(a) $\underline{Z}_{s,1}$ (b) $\underline{Z}_{s,2}$

Fig. 3. Scalar impedance hologram of feed 1 (a) and 2 (b) at 20 GHz.

III. Physical Implementation of Multi-Feed Holograms

For the physical implementation of each scalar impedance hologram, a pixel mapping process is introduced. To that end, the antenna aperture is divided in sub-wavelength sized unit cells (UC) ($\approx \frac{\lambda_0}{10}$) to mimic a homogeneous surface structure. Each UC is assigned to a pixel geometry to realize the scalar impedance, whose geometric parameters control the impedance value. In case of the multi-feed antenna with $N = 2$ feeding points, there are two different pixel geometries for each UC obtained by the hologram synthesis for feed 1 and feed 2. An example UC with the individual pixel geometries is illustrated in Fig. 4. The pixel structure required by feed 1 is shown on the left and the pixel of feed 2 on the right. For the realization of one pixel geometry in the shared UC, a merge has to be conducted.

A. Arithmetic Average

The state-of-the-art approach for designing multi-feed antennas is to average the N impedance tensor holograms resulting from the IBC [5]:

$$\overleftrightarrow{\underline{Z}}_{\text{avg}}(x,y) = \frac{1}{N}\sum_{n=1}^{N}\overleftrightarrow{\underline{Z}}_n(x,y) \qquad \forall n \in \mathbb{N}\,. \tag{4}$$

This corresponds to an averaging of the N discrete impedance tensors for each UC. For the consideration from Fig. 4, the merged UC corresponds to the average of the individual UC impedance tensors $\overleftrightarrow{\underline{Z}}_{\text{UC},1}$ and $\overleftrightarrow{\underline{Z}}_{\text{UC},2}$. From the discrete impedance tensor $\overleftrightarrow{\underline{Z}}_{\text{UC,avg}}$ of the exemplary UC, the pixel geometry is determined. This procedure is performed for each UC on the antenna aperture. However, this methodology neglects the incident angle of the SW w.r.t. the UC. This leads to the fact that the lowest impedance error for each feed cannot be realized by the merged impedance tensor. An approach considering the angular dependence is presented in the following.

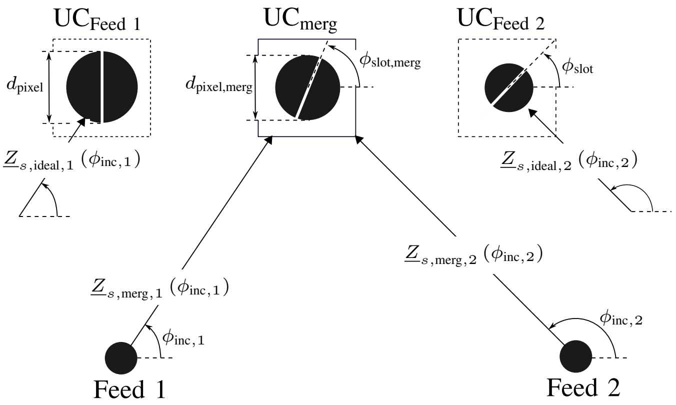

Fig. 4. Incident angle dependent merging method for an exemplary UC and an anisotropic pixel geometry.

B. Angle Dependent Impedance

In this contribution, a circular pixel geometry with a slot is used to realize the anisotropic impedance tensor on the aperture. The slot angle ϕ_{slot} controls the TM and TE components of the surface currents and thus is related to the anisotropy of the impedance tensor $\overleftrightarrow{\underline{Z}}_n$. By scaling the pixel diameter d_{pixel}, the isotropic portion of the impedance tensor can be controlled. In Fig. 4, the novel concept of merging two pixel geometries is illustrated considering the incident angle of the SW on a UC. The proposed synthesis algorithm first determines the slot angle $\phi_{\text{slot,merg}}$ of the shared unit cell UC_{merg} by averaging $\phi_{\text{slot,1}}$ and $\phi_{\text{slot,2}}$, thus the error for the anisotropy of UC_{merg} is minimized. The diameter $d_{\text{pixel,merg}}$ is chosen to minimize the scalar impedance error for each i-th UC, which can be defined as

$$\Delta Z_s(i) = \sum_{n=1}^{N=2} \left| \underline{Z}_{s,\text{ideal},n}(i) - \underline{Z}_{s,\text{merg},n}(i) \right| \quad \forall\, i \wedge n \in \mathbb{N}\,. \tag{5}$$

The scalar impedances $\underline{Z}_{s,\text{ideal},n}$ and $\underline{Z}_{s,\text{merg},n}$ depend on the incident angle on $\text{UC}_{\text{merged}}$ from the respective feed as can be seen in Fig. 4. Minimizing the impedance error ΔZ_s realizes the optimal pixel diameter for the shared UC leading to a lower deviation in the individual objective electric field distribution from (3) for each feeding point. This optimization of the pixel structure of each i-th UC can also be understood as a local optimization of the holographic multi-feed antenna.

C. Optimization with a Genetic Algorithm

Depending on the feed positions (x_1, y_1) and (x_2, y_2) in Fig. 1, the hologram synthesis results in different impedance holograms, since the maximum of the surface current is located in the origin of the respective feed position. Therefore, the merged impedance hologram becomes a function of the feed positions, and this opens another degree of freedom in the design process of the multi-feed antenna. In addition to the local optimization of all UCs, a global optimization of the feed positions can be performed. The goal of this global optimization is to minimize the global impedance error, which can be described as

$$e = \sum_{i=1} \Delta Z_s(i) \ \ \forall\, i \in \mathbb{N}\,. \tag{6}$$

Therefore, a genetic algorithm is integrated in the design process of the holographic multi-feed antenna to find the optimal feed positions and minimizes the global impedance error e.

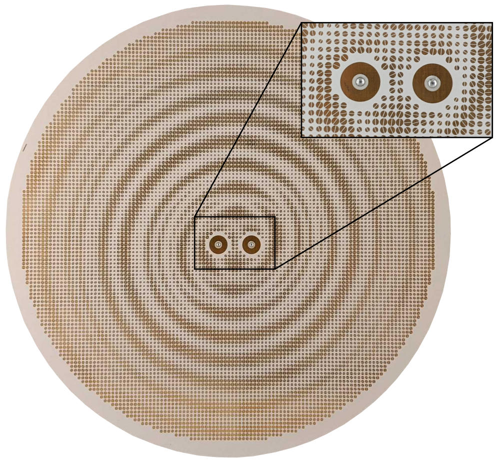

Fig. 5. Photograph of the fabricated holographic multi-feed antenna with the surface wave launchers (SWL) of each feed.

IV. Realization and Measurement

A multi-feed antenna with two feeding points was realized, based on the proposed synthesis algorithm for multi-feed holographic LW antennas. A $1.57\,\text{mm}$-thick Rogers 3003 substrate with a relative permittivity of $\varepsilon_r = 3$ and a loss tangent 0.001 is chosen to suppress higher order SW modes. The two feed positions $(x_1 = -6\,\text{mm}, y_1 = -8\,\text{mm})$, $(x_2 = 12\,\text{mm}, y_2 = -8\,\text{mm})$ where determined by the genetic

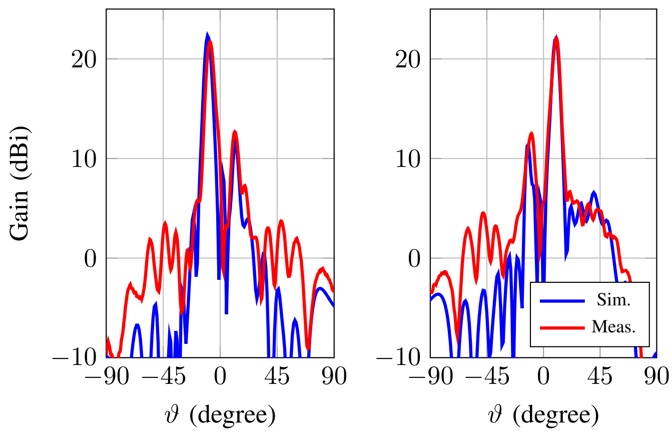

(a) Feed 1 (b) Feed 2

Fig. 6. Simulated and measured radiation patterns of the proposed multi-feed antenna at $20\,\text{GHz}$.

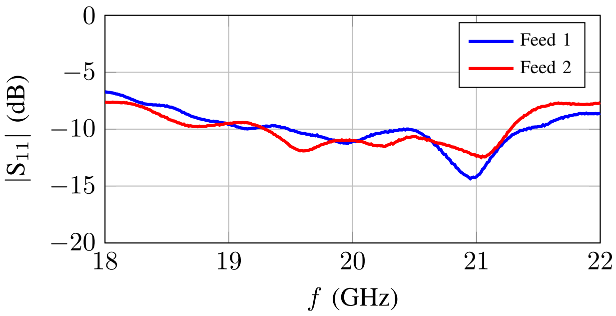

Fig. 7. Measured reflection coefficient of the multi-feed antenna at 20 GHz.

algorithm optimization with the goal to minimize the global impedance error. Both feeds are excited by a surface wave launcher (SWL) depicted in Fig. 5. A via connects each SWL with a coaxial connector on the bottom side of the antenna. The aperture consists of 10 000 UCs with a size of $2\,\text{mm} \times 2\,\text{mm}$. This results in a circular aperture with a diameter of $240\,\text{mm}$. The pixel geometry is set to a circular one with a slot. The elevation angle of the main beam is at $\vartheta_{0,1} = -10°$ and $\vartheta_{0,2} = 10°$, at 20 GHz. In Fig. 6, the simulation and measurement results of the multi-feed antenna are presented for the elevation angles $\vartheta = \pm 90°$ for both feeds and show a good agreement. The antenna gain of the realized multi-feed antenna has measured to 21.7 dBi for feed 1 and 22.1 dBi for feed 2. This results in a maximum deviation between measurement and simulation of 0.6 dB. Both feeds have a 3 dB-beamwidth (BW) of 6.0° and a minimum sidelobe level of 9.0 dB. The higher side lobe in each radiation pattern occur at the mainbeam elevation angle from the other feed. This is due to a crosstalk between the feeding points and can be solved by increasing their distance. The measured reflection coefficient from 18 GHz to 22 GHz is illustrated in Fig. 7. For the designed frequency of 20 GHz, feed 1 and 2 have a reflection coefficient of −11.1 dB and −11.0 dB, respectively.

V. Conclusion

In this paper an incident angle dependent synthesis process for holographic multi-feed antennas is presented. A multi-feed antenna with two feeding points was realized at 20 GHz, which shows good agreement between the simulation and measurement results. With the help of a genetic algorithm, a global optimization was performed exploiting the degree of freedom of the feed positions. The minimum measured antenna gain for both radiation pattern is 21.7 dBi, and the minimum SLL is 9.0 dB.

References

[1] G. Minatti, F. Caminita, E. Martini, M. Sabbadini, and S. Maci, "Synthesis of Modulated-Metasurface Antennas With Amplitude, Phase, and Polarization Control," *IEEE Transactions on Antennas and Propagation*, vol. 64, no. 9, pp. 3907–3919, 2016.

[2] G. Minatti, M. Faenzi, E. Martini, F. Caminita, P. D. Vita, D. González-Ovejero, M. Sabbadini, and S. Maci, "Modulated Metasurface Antennas for Space: Synthesis, Analysis and Realizations," *IEEE Transactions on Antennas and Propagation*, vol. 63, no. 4, pp. 1288–1300, Apr. 2015.

[3] G. Minatti, S. Maci, P. De Vita, A. Freni, and M. Sabbadini, "A circularly-polarized isoflux antenna based on anisotropic metasurface," *IEEE Transactions on Antennas and Propagation*, vol. 60, no. 11, pp. 4998–5009, 2012.

[4] T. Galler, T. Frey, C. Waldschmidt, and T. Chaloun, "High-Gain Millimeter-Wave Holographic Antenna in Package using Glass Technology," *IEEE Antennas and Wireless Propagation Letters*, pp. 1–5, 2020.

[5] D. González-Ovejero, G. Minatti, G. Chattopadhyay, and S. Maci, "Multibeam by Metasurface Antennas," *IEEE Transactions on Antennas and Propagation*, vol. 65, no. 6, pp. 2923–2930, Jun. 2017.

[6] B. H. Fong, J. S. Colburn, J. J. Ottusch, J. L. Visher, and D. F. Sievenpiper, "Scalar and Tensor Holographic Artificial Impedance Surfaces," *IEEE Transactions on Antennas and Propagation*, vol. 58, no. 10, pp. 3212–3221, Oct. 2010.

ISBN 978-3-9820397-2-5